Overheated metastable states in pulsed laser action on ceramics

V. I. Mazhukin
Institute of Mathematical Modeling, Russian Academy of Sciences, Miusskaya Square, 4, 125047 Moscow, Russia, CIS

I. Smurov
Ecole Nationale d'Ingénieurs de Saint-Etienne, 58, Rue Jean Parot, 42023 Saint-Etienne Cedex 2, France

G. Flamant[a)]
Institut de Science et de Génie des Matériaux et Procédés, C.N.R.S., B.P. 5, 66125 Font-Romeu Cedex, France

(Received 2 March 1994; accepted for publication 3 April 1995)

Volume overheating of solid and liquid phases in pulsed laser evaporation of superconducting ceramics is analyzed by numerical simulation. The mathematical model includes the processes of heating (with a volume energy release), melting-solidification, and evaporation. It is shown that the maximum values of overheating of the solid phase (with respect to its melting point) exceed 100 degrees and those of the liquid phase exceed several hundred degrees (with respect to the surface temperature). The times of existence of these metastable states are tens and hundreds of nanoseconds, respectively. The dynamics of the processes are analyzed in a wide range of variation of the absorption coefficient (i.e., laser wavelength). It is shown that the probability of explosive decay of the metastable states in the solid phase increases with laser wavelength, whereas for the metastable states in the liquid phase the overheating parameters exhibit a maximum versus laser wavelength. © *1995 American Institute of Physics.*

I. INTRODUCTION

The laser technique of thin-film deposition is considered to be one of the most promising and universal methods for deposition. It has already been applied to nearly 130 different materials.[1,2] It has been shown experimentally that the coating quality depends on the stability of the laser evaporation of the target, which in turn depends on the beam parameters: intensity, pulse duration, radiation wavelength, as well as heat transfer and optical properties of the evaporated materials.[1,2]

Pulsed laser deposition (PLD) of superconducting ceramics[3–5] has been found to be rather sensitive to the process parameters. The behavior of superconducting ceramics during PLD is one of the most complicated problems of laser action on condensed media, it includes practically all the basic phenomena: heating, melting, evaporation, plume formation, laser-beam–plume interaction, etc. Laser evaporation of metals and ceramics is a first-order transition (together with melting) whose dynamics significantly affects the stability of the materials removal. At the same time, the mechanism leading to the formation of temperature fields in superconducting ceramics has certain peculiarities because of the volume character of laser energy release.

When analyzing theoretically PLD of ceramics, it becomes necessary to consider simultaneously a variety of physical processes. Among them is the poorly studied problem of connections between phase transformations and metastable states of matter. Rapid phase transformations are known to be always accompanied by emergence of metastable states. To date considerable experimental and theoretical knowledge on overheating and undercooling of liquid and gaseous phases during evaporation, crystallization, and condensation has been accumulated.[6–11] Less studied is the problem of the occurrence of overheated states in solids, which are associated with laser melting[12–15] and sublimation.[16–19] Theoretical analysis performed in some earlier works[20,21] either excluded the possibility of overheating of solid materials or considered it as negligible. The situation has been changed crucially with the advent of powerful pulsed energy sources which could operate[22,23] in regimes for which the energy supply time is comparable with phase transformation times.

Different aspects of laser evaporation during the bulk heating of dielectric liquids (water, acetone, ethanol) have been studied in a large number of experimental and theoretical works (for example, Refs. 24–26). Since thermal diffusivity a and absorption κ are relatively small, the condition of bulk heating of a liquid during laser evaporation $V_{kv}/a\kappa \geqslant 1$ is realized even at comparatively low evaporation rates $V_{kv} \approx 1$ cm/s (Ref. 24) (V_{kv} is velocity of the liquid-vapor interface). The influence of an overheated metastable region in a liquid is revealed by the competition between surface evaporation and volume boiling of the liquid phase.

Very few studies are devoted to conditions for the emergence of overheated metastable states in the solid phase, which accompany laser melting.[22,23] In fact, no comprehensive study of the influence of a strong overheating of the solid phase on the melting process has been made.

The present work deals with the processes of pulsed melting and evaporation of superconducting ceramics of the $YBa_2Cu_3O_{7-x}$ type by laser radiation with an intensity which is typically used for superconducting films deposition in a nanosecond range of pulse duration. Methods of numerical simulation are applied in order to study the following:

[a)]Author to whom correspondence should be sent.

 0021-8979/95/78(2)/1259/12/$6.00

(a) the formation of temperature fields while accounting for the dynamics of phase transformations and volume energy release;
(b) the role and influence of overheated metastable states in solid and liquid phases on the melting and on the evaporation processes;
(c) the peculiarities of phase fronts dynamics which depend on the optical properties of the material.

II. PHYSICAL AND MATHEMATICAL MODEL

Theoretical analysis of the pulsed laser action on ceramics which account for phase transformations is a rather complicated problem. Therefore, in order to solve this problem one has to resort to various simplifying assumptions.

A. Principal physical assumptions

1. Thermophysical properties of metastable states

The properties of overheated liquids and solids essentially depend on the depth of penetration into the metastable region. When the penetration is deep, singularities may arise close to the spinodal in thermodynamical characteristics of the material. These singularities[27] are in the form of, for example, unlimited increase in thermal capacity C_p and vanishing thermal diffusivity a. When the penetration into the metastable region is not deep (with respect to the binodal), overheated liquids show no peculiarities.[28] In laser evaporation of strongly absorbing condensed media, such as metals, metastability of the overheated phase is not revealed up to relatively high temperatures $T \approx 0.85 T_c$,[24] where T_c is the temperature of the substance at its critical point.

On the basis of these data it can be assumed that metastable states accompanying phase transformations in ceramics do not affect heat transfer and optical properties of the material.

2. Lifetime of metastable states

One of the main properties of metastable states is their finite lifetime. Decay of metastable states is, as a rule, due to processes of nucleation of the competing phase. Problems of thermodynamic stability and dynamics of the decay of metastable states are of special interest and require a separate analysis. When applied to laser action on condensed media, these problems can be reduced to determine the relative role of surface and volume mechanisms of evaporation and melting. The mathematical model used in the present article is based on the assumption that overheated metastable states have a stable behavior during laser action, and the processes of surface melting and evaporation are the main mechanisms of the phase transformations solid-liquid and liquid-vapor. Thus, the processes of nucleation and related processes of volume melting and evaporation are beyond the scope of this work. This allows one to be able to simplify the problem, without this assumption the explosive decay of metastable phases must be taken into account. At present there are no fully developed theoretical models that could be used as a basis for a quantitative analysis of such phenomena.

3. Averaged heat-transfer properties

Generally, ceramics are heterogeneous materials. Their heat-transfer properties are not well known, especially at high temperatures. Here, ceramics are considered as homogeneous materials characterized by averaged heat-transfer properties.

4. 1D approximation

All the processes in the irradiation zone are considered to be one dimensional. The required condition of the small length of the heat effected zone as compared to the irradiation zone diameter is supposed to be respected.

B. Mathematical model

Theoretical analysis of the dynamics of the first-order phase transition leads to the different versions of the Stefan problem,[29] which in mathematical physics implies a whole class of problems with moving boundaries, described by parabolic or elliptic equations. In its general formulation the Stefan problem can be reduced to a boundary-value problem with piecewise continuous coefficients having the first-order breaks on *a priori* unknown moving surfaces.

Mathematical description of the processes of laser heating (melting-solidification and evaporation of superconducting ceramics) is made within the framework of the combined version of the Stefan problem including the dynamics of both phase fronts: melting-solidification and evaporation. The proposed mathematical model is a boundary-value problem for the heat-transfer equation with two moving phase boundaries solid-liquid $\Gamma_{sl}(t)$ and liquid-vapor $\Gamma_{kv}(t)$. Volume heating of the solid and liquid phases is taken into account with the help of the term $\partial G/\partial x$ in the heat-transfer (1) and the radiation-transfer (2) equations,

$$\left(C_p \rho \frac{\partial T}{\partial t} = \frac{\partial}{\partial x} \lambda(T) \frac{\partial T}{\partial x} - \frac{\partial G}{\partial x} \right)_k , \tag{1}$$

$$\left(\frac{\partial G}{\partial x} + \kappa G = 0 \right)_k , \quad k = s, l, \quad t > 0, \tag{2}$$

solid phase: $x_0 < x < \Gamma_{sl}(t)$;

liquid phase: $\Gamma_{sl}(t) < x < \Gamma_{kv}(t)$.

1. Melting-solidification phase transition

In the classical version of the Stefan problem for the description of melting-solidification phase transitions at the interface boundary $\Gamma_{sl}(t)$ the differential condition is used,

$$x = \Gamma_{sl}(t): \quad \lambda_s \frac{\partial T_s}{\partial x} - \lambda_l \frac{\partial T_l}{\partial x} = p_s L_m V_{sl}, \tag{3}$$

from which the velocity of the front movement V_{sl} is determined. Besides condition (3), we must prescribe another condition associated, in the general case, with the kinetics of phase transition. In the classical version of the Stefan problem it is supposed that at the interface boundary the temperature T_{sl} is continuous and equal to the equilibrium transition temperature T_m,

$$T_{sl} = T_s = T_l = T_m . \tag{4}$$

In many cases the equilibrium phase transition temperature T_m can be considered to be a constant value. The phenomenological condition (4) does not contain explicitly the phase transition under nonequilibrium, the application of this condition implies that melting begins immediately upon reaching the transition temperature T_m. Thus, overheating of solid body surface is excluded from consideration. This approach can be referred as traditional. For example, in a well-known monograph[30] it is pointed out that overheating of a solid free surface is not, generally speaking, realized.

The nonequilibrium phase transformation may be taken into account explicitly in the so-called kinetic condition (5), connecting the velocity of the interface boundary V_{sl} with its temperature T_{sl}. According to the classical theory,[10,12,13,31] this condition can be written in a simplified way as

$$V_{sl}(T_{sl})=C_1 \exp\left(-\frac{U}{kT_{sl}}\right)\left[1-\exp\left(-\frac{L_m\Delta T}{kT_mT_{sl}}\right)\right], \tag{5}$$

where C_1 is the constant depending on the material, U is the activation energy, $\Delta T=T_m-T_{sl}$. Using the kinetic condition (5), where the phase transition nonequilibrium is explicitly present, instead of equality (4) leads to the phase boundary movement in melting/solidification processes under overheating or undercooling (ΔT) only.

It should be noted that other approaches[14,32] are also used to formulate the kinetic condition. At present, however, there is no generally accepted approach. The question of whether to use the equilibrium models (1)–(4) or the nonequilibrium models (1)–(3),(5) to describe pulsed modes of action is still under discussion.

In the present article the mathematical models (1)–(3) with the equilibrium condition (4) is used to simulate melting-solidification processes. As noted above, the application of the phenomenological condition (4) involves the absence of the solid phase surface overheating during melting and liquid phase surface undercooling during solidification. However, in the case of volume heating, as it is be shown later, the overheating of the solid phase is the necessary condition for the Stefan problem to be applicable for description of melting process dynamics.

2. Surface evaporation

To describe mathematically the process of intensive surface evaporation, the well-known approach is used where the plane boundary temperature T_{sur} depends logarithmically on the front velocity.[33] Intensive evaporation gives rise to a strongly nonequilibrium Knudsen layer at the interface. Usually in evaporation problems the Knudsen layer is a gas dynamic gap, for which three laws of conservation (mass, momentum, and energy) and two additional relations describing the nonequilibrium degree of the phase transformation are written. Several approximate models of the Knudsen layer were developed.[24,34–37] Assuming that evaporation occurs into vacuum or in a medium whose pressure P_0 is much less than the saturated vapor pressure P_H $(T_{sur})\gg P_0$, any one from the above-mentioned models can be used. In the present article the relations reported in Ref. 36 are used. In case of volume heating of a condensed medium the boundary conditions on the surface being evaporated have the form

$$x=\Gamma_{kv}: \quad -\lambda_k\frac{\partial T_{sur}}{\partial x}=\rho_kL_vV_{kv}-\epsilon\sigma T_{sur}^4, \tag{6}$$

$$\rho_kV_{kv}=\rho_v(V_{kv}-u), \tag{7}$$

$$P_k+\rho_kV_{kv}^2=P_v+\rho_v(V_{kv}-u)^2, \tag{8}$$

$$T_v=T_{sur}\left\{\left[1+f^2\left(\frac{\gamma-1}{\gamma+1}\right)^2M^2\right]^{1/2}-f\left(\frac{\gamma-1}{\gamma+1}\right)M\right\}^2, \tag{9}$$

$$\rho_v=\frac{1}{2}\rho_H\left[\left(\frac{T_{sur}}{T_v}\right)^{1/2}\left((\gamma M^2+1)\exp(b^2M^2)\operatorname{erfc}(bM)-\frac{4f}{\pi}M\right)+\frac{T_{sur}}{T_v}\left[1-2fM\exp(b^2M^2)\operatorname{erfc}(bM)\right]\right], \tag{10}$$

$$M=\frac{u}{u_c}, \quad u_c=(\gamma RT_v)^{1/2}, \quad b=\left(\frac{\gamma}{2}\right)^{1/2}, \quad f=\left(\frac{\pi\gamma}{8}\right)^{1/2},$$

$$\rho_H=\frac{P_H}{RT_{sur}}, \quad P_H=P_b\exp\left[\frac{L_v}{RT_b}\left(1-\frac{T_b}{T_{sur}}\right)\right].$$

In case of surface heating the energy balance on the irradiated surface is written as

$$-\lambda_k\frac{\partial T_{sur}}{\partial x}=\rho_kL_vV_{kv}+G_{sur}-\epsilon\sigma T_{sur}^4, \tag{11}$$

where

$$G_{sur}=A(T_{sur})G.$$

Note that the x axis is oriented along the outward drawn normal to the irradiated body surface. Other conditions remain unchanged.

The terms are defined as follows: a thermal diffusivity; $A(T_{sur})$ surface absorptivity; G energy density flux; G_{sur} absorbed energy density flux; G_0 maximum value of incident energy density flux; L_m latent heat of melting; L_v latent heat of evaporation; M Mach number; P pressure; R universal gas constant; t time; $-t_0,t^j$ the limits of time variation; $T(x,t)$ temperature; T_0 initial temperature; T_m melting point; u vapor velocity; V_{sl} velocity of solid-liquid interface; V_{kv} velocity of evaporation interface; x spatial coordinate; x_0,x_1 the limits of coordinate variation; γ the ratio of specific heat at constant pressure to that at constant volume; Γ_{sl} solid-liquid interface; Γ_{kv} evaporation interface; κ absorption coefficient; λ thermal conductivity; ρ density; ϵ emissivity: The subscripts indicate the following: b is the boiling point; H saturated vapor; l liquid; s solid; v gas phase; k condensed phase (solid or liquid); sur surface; ν laser radiation.

III. METHOD OF THE SOLUTION

To prove the validity of the obtained nontraditional results, we present the details of our numerical method of solution. Note: The simulation of the Stefan-type problems with the volume energy release should be done by the explicit tracking of phase front positions and not by the widely used treatment of latent heat evolution.

A. Basis of the dynamic adaptation method

The principal difficulty for solving the Stefan-type problems is connected with the presence of moving interface boundaries whose positions are not known in advance and must be determined while solving the problem. Since the solution region is unknown and changes with time, some difficulties arise when constructing spatial computational grids. These difficulties can be overcome with the help of the dynamic adaptation method[38–40] where the problem of computational grids construction is formulated on the differential level. It means that in the mathematical model one part of differential equations describes physical processes, while the other part describes the behavior of the grid nodes.[39] The dynamic adaptation method is based on the procedure of transition to an arbitrary transient coordinate system with the help of the sought-for solution. The transition to a transient coordinate system enables one to avoid problems associated with moving boundaries. This is done at the expense of increasing the number of unknown quantities, since now it is not only the grid functions that are sought for but the coordinate nodes as well. Arbitrary choice of a transient coordinate system makes it possible, in general, to solve problems with any number of moving boundaries. Moreover, it makes the method universal and simple, since the transition to a required coordinate system is performed by choosing a particular transformation function Q depending in the general case on the solution.[38–40] With the help of this function it is easy to make a desirable grid node distribution, depending on the special features of the sought-for solution. Among the examples of the method applications are: propagation of large gradients, strong gaps, contact, and phase boundaries.

B. Application of dynamic adaptation method to the motion of melting-solidification and evaporation fronts

Let us write the mathematical models (1)–(4) and (6)–(10) in an arbitrary transient coordinate system. Let (x,t) be the initial independent variables, and (q,τ) be the independent variables in the new coordinate system. The transition from one coordinate system to the other is carried out by substituting variables in the general form $x=f(q,\tau)$, $t=\tau$, which has the inverse nondegenerate transformation $q=\Phi(x,t)$, $\tau=t$. Partial derivatives of the dependent variables are expressed as

$$\frac{\partial}{\partial t}=\frac{\partial}{\partial \tau}+\frac{\partial q}{\partial \tau}\frac{\partial}{\partial q}=\frac{\partial}{\partial \tau}-\frac{\partial x}{\partial \tau}\frac{\rho}{\Psi}\frac{\partial}{\partial q}=\frac{\partial}{\partial \tau}+\frac{Q}{\Psi}\frac{\partial}{\partial q},$$

$$\frac{\partial}{\partial x}=\frac{\partial q}{\partial x}\frac{\partial}{\partial q}=\frac{\rho}{\Psi}\frac{\partial}{\partial q},\quad \Psi=\frac{\partial x}{\partial q}\rho,$$

where $\partial x/\partial\tau=-Q/\rho$ is the coordinate system velocity, Q is the arbitrary function depending in the general case on the sought-for solution, ψ is the metric coefficient or the transformation coefficient indicating how many times the initial region changes with time.

Using the given substitution of partial derivatives, we can write the mathematical models (1)–(4) and (6)–(10) in variables (q,τ) and represent the differential equations in the divergent form

$$\left(\frac{\partial(H\Psi)}{\partial\tau}=-\frac{\partial W}{\partial q}-\frac{\partial(Q\Psi)}{\partial q}-\frac{\partial G}{\partial q}\right)_k, \tag{12}$$

where $H=C_pT$ and $W=-(\rho\lambda/\Psi)(\partial T/\partial q)$,

$$\left(\frac{\partial G}{\partial q}+\frac{\kappa\Psi}{\rho}G=0\right)_k, \tag{13}$$

$$\left(\frac{\partial\Psi}{\partial\tau}=-\frac{\partial Q}{\partial q}\right)_k,\quad \left(\frac{\Psi}{\rho}=\frac{\partial x}{\partial q}\right)_k,\quad k=s,l, \tag{14}$$

$$q_0<q<\Gamma_{sl}(t),\quad \Gamma_{sl}(t)<q<\Gamma_{kv}(t),\quad \tau>0.$$

Initial and boundary conditions are

$$\tau=0:\quad T(q,0)=T_0,$$

$$q=q_0:\quad \frac{\lambda\rho}{\Psi}\frac{\partial T}{\partial q}=0,\quad Q=0, \tag{15}$$

$$q=\Gamma_{sl}:\quad T_{sl}=T_m,\quad Q_{sl}=-\frac{W_s-W_l}{L_m},\quad Q_{sl}=-\rho_sV_{sl}, \tag{16}$$

$$q=\Gamma_{kv}:\quad \frac{\lambda_k\rho_k}{\Psi_k}\frac{\partial T_{sur}}{\partial q}=L_vQ_{kv}+\epsilon\sigma T_{sur}^4, \tag{17}$$

$$\rho_kV_{kv}=\rho_v(V_{kv}-u),\quad Q_{kv}=-\rho_kV_{kv}, \tag{18}$$

$$P_k+\rho_kV_{kv}^2=P_v+\rho_v(V_{kv}-u)^2, \tag{19}$$

$$T_v=T_{sur}\left\{\left[1+f^2\left(\frac{\gamma-1}{\gamma+1}\right)^2M^2\right]^{1/2}-f\left(\frac{\gamma-1}{\gamma+1}\right)M\right\}^2, \tag{20}$$

$$\rho_v=\frac{1}{2}\rho_H\left[\left(\frac{T_{sur}}{T_v}\right)^{1/2}\left((\gamma M^2+1)\exp(b^2M^2)\operatorname{erfc}(bM)-\frac{4f}{\pi}M\right)+\frac{T_{sur}}{T_v}\left[1-2fM\exp(b^2M^2)\operatorname{erfc}(bM)\right]\right], \tag{21}$$

$$M=\frac{u}{u_c},\quad u_c=(\gamma RT_v)^{1/2},$$

$$b=\left(\frac{\gamma}{2}\right)^{1/2},\quad f=\left(\frac{\pi\gamma}{8}\right)^{1/2},$$

$$\rho_H=P_H/RT_{sur},\quad P_H=P_b\exp\left[\frac{L_v}{RT_b}\left(1-\frac{T_b}{T_{sur}}\right)\right].$$

Equation (14) is the inverse transformation equation. In this equation the function Q, as noted above, depends on the special features of the sought-for solution. In general case a great freedom of choice is allowed to determine the Q function and this task should be done by a user. Without going into detail how one chooses the function Q (a special analysis of this question is given in Ref. 40), we can point out that for the moving boundary problems the function of Q

$= -D(\partial\Psi/\partial q)$ is suitable. With an optimum value of the coefficient D this function provides a uniform distribution of nodes at any moment.

Numerical solution of the mathematical models (12)–(21) was performed with the LASTEC-1 software.[41–43] In a usual way the space of the continuous argument functions is substituted by the space of the discrete argument functions (grid functions), and the system of differential equations (12)–(14) is approximated by finite difference relations expressed as a system of algebraic equations. The entirely implicit conservative scheme with the approximation of the order of $O(\Delta\tau+h^2)$ (where $\Delta\tau$, h are the steps of τ and q variables used for computation).

IV. RESULTS AND DISCUSSION

Analysis of experimental and theoretical data[3,44–46] on heat transfer λ, C_p, ρ, and optical A,κ properties of $YBa_2Cu_3O_{7-x}$ ceramics revealed their comparatively weak dependence on temperature. According to these data the thermal diffusivity of YBaCuO ceramics is $a\sim(2-5)10^{-2}$ cm^2/s. Thus, the thermal properties of ceramics are close to those of dielectrics $a\sim10^{-3}-10^{-2}$ cm^2/s. At the same time the optical characteristics vary strongly when changing wavelength of incident radiation.[3] In accordance with experimental dependence $\kappa(\lambda_\nu)$ given by Ref. 3 the absorption coefficient κ ranges from $\kappa\approx8\times10^5$ cm^{-1} for the radiation wavelength $\lambda_\nu=0.2$ μm to $\kappa\approx10^4$ cm^{-1} for the radiation wavelength $\lambda_\nu\geqslant1$ μm. As a result, ceramics can absorb laser radiation depending on radiation wavelength either as metals ($\kappa\leqslant5\times10^5$ cm^{-1} in the short-wavelength range) or as dielectrics ($\kappa\simeq10^4$ cm^{-1} in the long-wavelength range).

It is well known[24] that energy absorption under pulsed laser irradiation can be either a volume or a surface phenomenon depending on the relation between thermophysical and optical parameters and irradiation regime. The surface heating condition for regimes without phase transformation can be written as $l_T\gg l_\nu$, i.e., the quantum mean free path $l_\nu\sim\kappa^{-1}$ is much smaller than the thermal influence length $l_T\sim(at)^{1/2}$. Volume energy absorption takes place in the opposite case $(at)^{1/2}\kappa\leqslant1$. The period of volume heating in ceramics can be of tens or hundreds of nanoseconds depending on the radiation wavelength.

For regimes with the first type phase transformations the volume energy absorption becomes appreciable when absorption depth $l_\nu\sim\kappa^{-1}$ becomes comparable with thermal influence length $l_T\sim a/V$, i.e., $a\kappa/V\leqslant1$ with V being evaporation front velocity. This condition can be written in the other form $V/a\kappa\geqslant1$ which is more convenient for further analysis. The considered ratio is the smallest for metals because of large κ and a, consequently the volume heating condition could be realized only for extremely high values of velocity $V>30$ m/s and for a quite small distance. On the other hand in dielectrics radiation absorption proceeds in the volume of material even for relative low velocities $V\sim0.01$ m/s. Ceramics behave intermediately between metals and dielectrics, and volume heating can occur for $V\sim0.1-1$ m/s. Consequently analysis of pulsed laser action on superconducting ceramics should be performed taking into account both volume and surface energy absorption. It is possible to expect that variation of the laser radiation dissipation mechanism may lead to qualitative changes in basic processes.

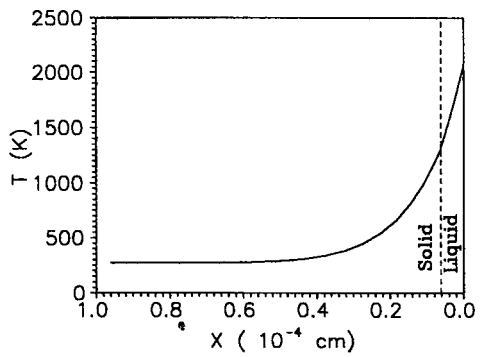

FIG. 1. Spatial temperature distribution a short time after the melting starts for surface energy absorption.

We performed simulation consecutively for each mechanism of laser radiation dissipation and we analyzed them. Taking into account the above consideration, mathematical simulation was carried out by two models:

(a) for surface heating (1),(3),(4),(7)–(11); and
(b) for volume heating (1)–(4),(6)–(10). The parameters were chosen to be the typical ones for PLD regimes of thin superconducting films. The temporal profile of laser pulse was assumed to have the Gaussian form by the variable t,

$$G(t)=G_0\exp\left[-\left(\frac{t}{\tau}\right)^2\right],$$

where $-\infty<t<+\infty$, τ is the pulse half-width at the half-height, $\tau=40$ ns, G_0 is the maximum intensity, $G_0=10^7$ W/cm^2. In the present simulation G_0 and τ remain the same for all the computation variants.

Heat-transfer and optical properties of the solid and liquid phase were assumed equal and independent of temperature and the values were chosen in accordance with experimental data,[3,44–46]

$$A=0.8,\quad T_m=1300\ \text{K},\quad T_b=2000\ \text{K},$$

$$C_p=5\times10^2\ \text{J/kg K},\quad L_m=2.5\times10^5\ \text{J/kg},$$

$$L_v=6\times10^6\ \text{J/kg},\quad \lambda=3\ \text{W/m K}.$$

A. Surface energy absorption

Spatial distribution of temperature $T(x)$ both in solid and liquid phase, Fig. 1, corresponds to a conventional distribution in low thermal conductivity materials under the action of a surface heat source. A low thermal conductivity leads to a strong spatial localization of temperature field. By the beginning of melting, the heated layer does not exceed 0.1 μm, which gives rise to high-temperature gradients in subsurface layers.

The presence of large temperature gradients is responsible for a high initial melting rate V_{sl}, Fig. 2. On the curve $V_{sl}(t)$ melting process corresponds to the negative branch, the solidification process corresponds to the positive one (x axis is oriented along the outward drawn normal to the

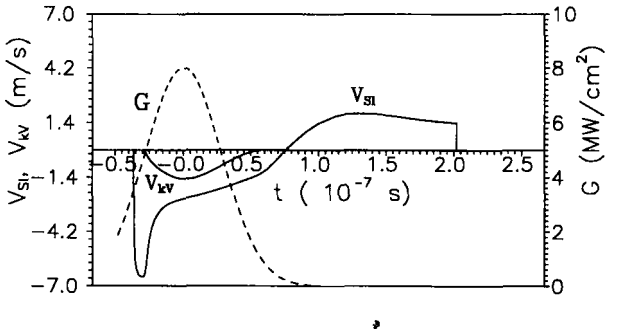

FIG. 2. Intensity of laser pulse G and phase front velocities V_{kv}, V_{sl} vs time for surface energy absorption.

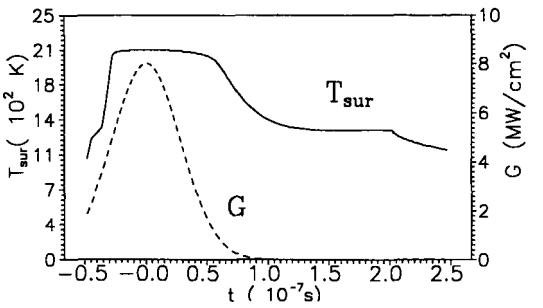

FIG. 4. Intensity of laser pulse G and surface temperature T_{sur} vs time for surface energy absorption.

irradiated body surface). After a short time, the melting front velocity reaches its maximum value $|V_{sl}^{max}|\approx 6$ m/s, and then it begins decreasing rapidly under the influence of the growing liquid phase. A further decrease of the melting rate is inhibited by the process of intensive surface evaporation whose maximum rate is up to $|V_{kv}^{max}| \approx 1.5$ m/s, Fig. 2. The high evaporation rate retards the liquid phase growth x_l, Fig. 3, which affects the decrease of $V_{sl}(t)$. The effect of the interaction of the phase fronts is particularly pronounced in the nonmonotonic behavior of the curve $x_l(t)$ which describes the dynamics of liquid phase thickness. After the end of intensive evaporation, the liquid phase thickness increases about 1.5 times. The maximum value is reached at the time when the laser radiation intensity decreases by about one order of magnitude.

The solidification process also proceeds at a rather high rate $|V_{sl}^{max}|\approx 2$ m/s, Fig. 2. The duration of this process is approximately equal to that of the melting process. On the curve $T_{sur}(t)$ (Fig. 4) the solidification process corresponds to the plateau with a practically constant temperature close to T_m. Thus, in the case of surface absorption of laser radiation melting-solidification process is described by the asymmetrical-in-amplitude and nearly symmetrical-in-time dependence of V_{sl} vs t.

The process of intensive evaporation is characterized by relatively high values of the rate $|V_{kv}^{max}| \approx 1.5$ m/s and recoil reaction pressure at the liquid surface $P_{sur}^{max}\approx 40$ bar. The time dependencies of $V_{kv}(t)$, Fig. 2, and $P_{sur}(t)$, Fig. 5, being slightly shifted, repeat the temporal profile of the radiation intensity $G(t)$. As it has been mentioned,[23,26] the surface of a liquid being evaporated turns out to be overheated with respect to the saturated vapor pressure. In the case of surface energy absorption this is the only display of metastability.

B. Volume energy absorption

In the case of laser radiation released in the bulk material, the behavior of the processes including the phase transitions, changes qualitatively, beginning from a certain value of the quantum mean free path $l_\nu \sim \kappa^{-1}$. The calculations show that appreciable duration (about $t\sim 1$ ns) of volume energy absorption in the solid phase during melting stage is reached with $\kappa\approx 2\times 10^5$ cm^{-1} at $\lambda\approx 0.3$ μm for the above-mentioned intensity and duration of laser pulse. Absorption coefficient κ decreases with radiation wavelength λ_ν, which leads to increasing of melting front velocity V_{sl} and duration of volume heating. The maximum duration is about 50 ns for $\lambda_\nu \geqslant 1.06$ μm and $\kappa \leqslant 2\times 10^4$ cm^{-1}.

The duration of the volume heating of liquid phase, which depends first of all on evaporation rate V_{kv}, becomes appreciable ($t\approx 10$ ns) for $\kappa\approx 5\times 10^5$ cm^{-1} at $\lambda\approx 0.2$ μm. The characteristic duration of volumetric heating exhibits a maximum with respect to the absorption coefficient (i.e., laser wavelength). The maximum value is about 100 ns for $\kappa = 6\times 10^4$ cm^{-1}. For smaller absorption coefficient (larger wavelength) this duration decreases strongly, and reaches 20 ns for $\kappa\approx 2\times 10^4$ cm^{-1}.

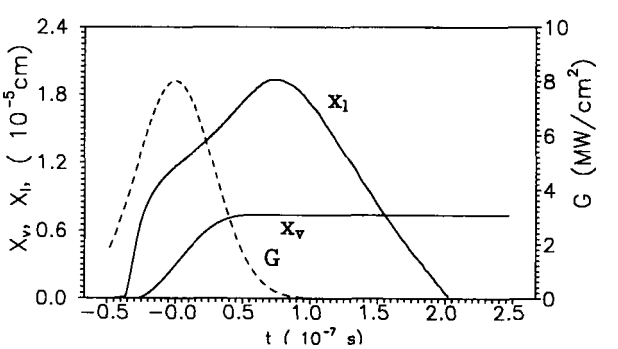

FIG. 3. Intensity of laser pulse G, thickness of liquid phase x_l, and thickness of evaporated layer x_v vs time for surface energy absorption.

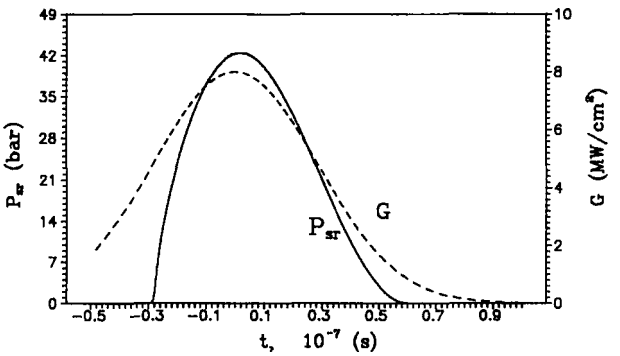

FIG. 5. Intensity of laser pulse G and recoil reactive pressure P_{sur} vs time for surface energy absorption.

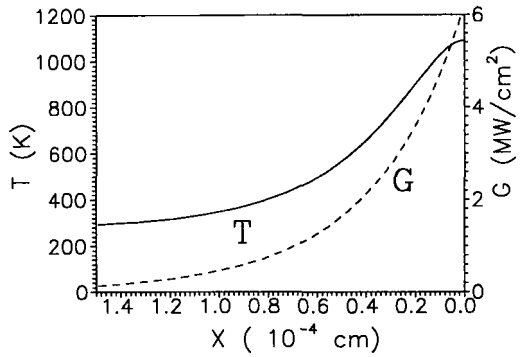

FIG. 6. Spatial distributions of absorbed energy intensity G and temperature T at the moment of liquid phase appearance for volume energy absorption (l_ν=3000 Å).

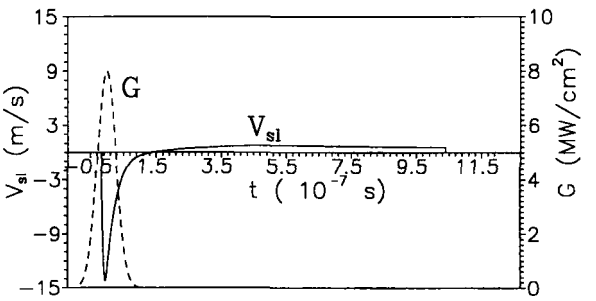

FIG. 8. Intensity of laser pulse G and velocity of melting-solidification front V_{sl} vs time for volume energy absorption (l_ν=3000 A).

Let us consider the influence of volume energy dissipation on the heat process dynamics. Calculations showed that for the small depth $l_\nu \approx 100$ Å, the process character does not practically differ from the surface energy absorption; however, with the increased free path l_ν the behavior of the process begins to change qualitatively. It is possible to note that these changes are due to the emergence of new metastable states (in volumes of the solid and liquid phases) whose role becomes greater with l_ν increasing. As a result, the melting process becomes dominant, the role of evaporation becomes less important, and, consequently, the liquid phase exists for an unusually long time. These effects are most evident in the absorption coefficient range $\kappa = 10^5 - 10^4$ cm^{-1} (mean free paths of 10^3–10^4 A), which corresponds to the laser wavelength $\lambda_\nu = 0.4$–0.9 μm;[3] for Nd:YAG laser ($\lambda_\nu = 1.06$ μm) $l_\nu \approx 1.3 \times 10^4$ A.

Increasing the quantum mean free path up to 3000 A results in a noticeable dissipation of the radiation energy in the bulk material. The spatial temperature profile in this case has a flat peak near the surface with a small temperature gradient, Fig. 6. Upon reaching the melting temperature T_m on the irradiated surface, the melting front begins to move into the material. Owing to moderate spatial temperature gradients, the initial melting rate becomes several orders less than the initial melting rate in the case of a surface heat source. Then under the combined action of the processes of melting and volume heating, the temperature maximum, Fig. 7, is formed in subsurface layers of the material. The development of this maximum is determined by the laser action parameters, and the material parameters κ, a, etc. The presence of the subsurface temperature maximum indicates that a certain volume of the solid phase is overheated with respect to the melting equilibrium temperature T_m.

Arising metastable states significantly affect the velocity of the melting front. The emergence of a temperature maximum at a certain distance from the boundary Γ_{sl} causes the change of the heat flow W_s (in the solid phase) direction, i.e., now it comes from inside the solid phase toward the melting front. As a result heat flows from the solid and liquid phases W_s and W_l are added together at the interface, and they are not subtracted one from the other, as in conventional cases.[29] The addition of the flows W_s and W_l results in a sharp increase in the melting rate whose maximum value $|V_{sl}^{max}| \approx 14$ m/s (Fig. 8) is more than twice that given in the case of a surface energy absorption, Fig. 2. High values of V_{sl} result in a fast growth of the liquid phase, Fig. 9, which absorbs ever greater portions of laser radiation. Overheating of the solid phase, then, decreases and vanishes completely.

Liquid phase heating causes an intensive surface evaporation, which in turn (with allowance for volume energy release in the depth of the liquid phase) leads to the formation of the second temperature maximum, Fig. 10. For some values of parameters both maxima can be observed simultaneously (Fig. 10). When considering evaporation kinetics the

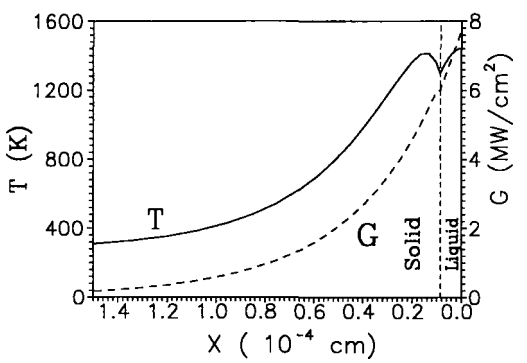

FIG. 7. Spatial distributions of absorbed energy intensity G and temperature T illustrating the appearance of solid-state overheating a short time after the melting starts (volume energy absorption, l_ν=3000 A).

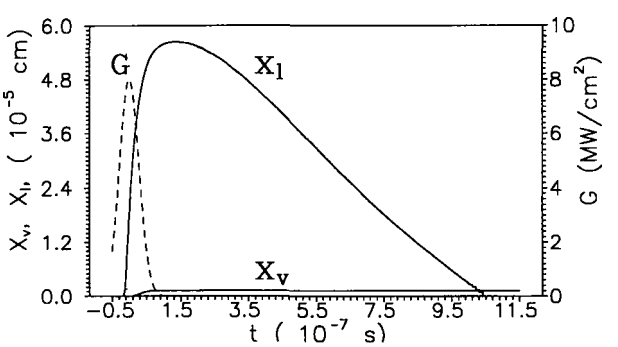

FIG. 9. Intensity of laser pulse G, thickness of liquid phase x_l, and thickness of evaporated layer x_v vs time for volume energy absorption (l_ν=3000 A).

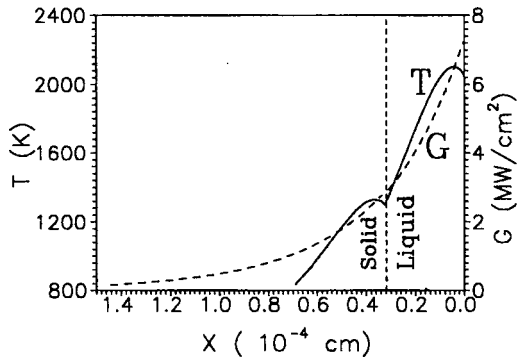

FIG. 10. Spatial distributions of absorbed energy intensity G and temperature T illustrating the existence of two subsurface temperature maxima: in solid phase and in liquid phase, a short time after the intensive evaporation starts (volume energy absorption, l_ν=3000 A).

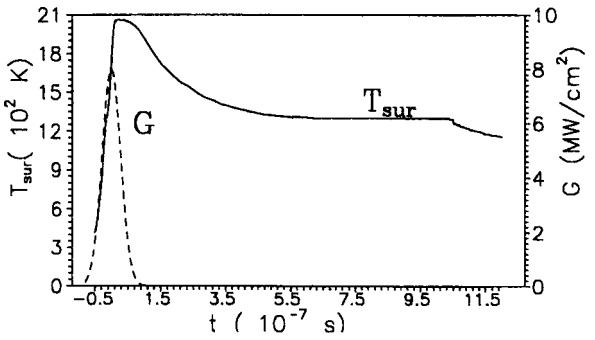

FIG. 12. Intensity of laser pulse G and surface temperature T_{sur} vs time for volume energy absorption (l_ν=3000 A).

temperature of the interface is not fixed; therefore, in the liquid phase not only the subsurface volume but the irradiated surface also is overheated with respect to the temperature corresponding to the saturated vapor pressure. The second feature is that the metastability of the liquid volume does not cause the acceleration of the evaporation front movement as compared to surface absorption. This observation is contrary to the solid phase overheating, where the metastable phase accelerates the melting front movement.

As compared with the evaporation rate calculated for surface energy absorption the maximum rate for volume absorption is reduced by about one order of magnitude (Fig. 11 indicates a value of 0.3 m/s). This phenomenon is due to the lower surface temperature in the case of radiation energy distribution in the bulk material. The reduction of the evaporation rate V_{kv} also leads to the lessening of its influence on the whole processes and, in particular, weakens interaction with the melting process.

At the same time due to the accumulation of energy in the subsurface layer the processes of melting-solidification and evaporation become extended in time. Thus, intensive evaporation begins after passing the maximum $G(t)$ and continues when the intensity $G(t)$ decreases by more than one order of magnitude (Fig. 12). As a result, the profiles of the evaporation rate $V_{kv}(t)$, Fig. 11, and pressure $P_{sur}(t)$, Fig. 13, are shifted to the right-hand side (they are later) with respect to the intensity maximum. The melting process continues for quite a long time after the end of the laser pulse. A typical feature of the solidification process when compared to the surface energy absorption is an extremely low velocity of the phase front propagation $|V_{sl}^{max}|\approx 0.55$ m/s, Fig. 8. Ultimately, the melting-solidification process is characterized by the curve $V_{sl}(t)$ which is highly asymmetric in amplitude and time, Fig. 8. The dependence of V_{sl} with time has a nearly unipolar shape.

Low evaporation and solidification rates lead to an unusually long lifetime of the liquid phase $\Delta t\sim 1$ μs. By comparison in case of surface absorption of laser radiation, the lifetime of liquid phase, as a rule, does not exceed pulse duration of more than two times for metals or three times for ceramics.[47]

C. General tendencies

In order to show general tendencies of the metastable states appearance and its influence on the dynamics of phase transitions, laser action over a wide range of mean free paths l_ν (from l_ν=0 to $l_\nu=5\times10^3$ A) is analyzed. The results are presented in Figs. 14–17.

Each point on these curves corresponds to the maximum (or final) value of analyzed function during thermocycle for a given value of absorption length (i.e., laser wavelength). For example, maximum absolute value of evaporation front velocity in Fig. 11 is about 0.3 m/s. So, this value is plotted on

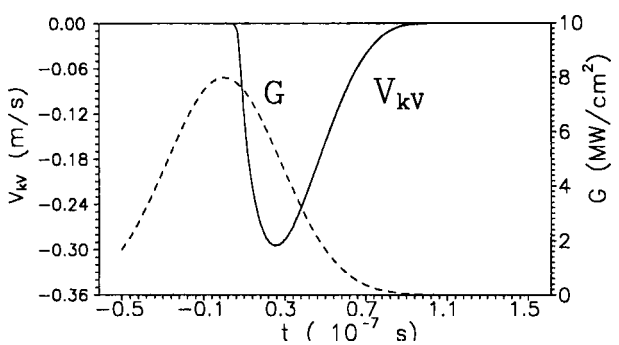

FIG. 11. Intensity of laser pulse G and evaporation front velocity V_{kv} vs time for volume energy absorption (l_ν=3000 A).

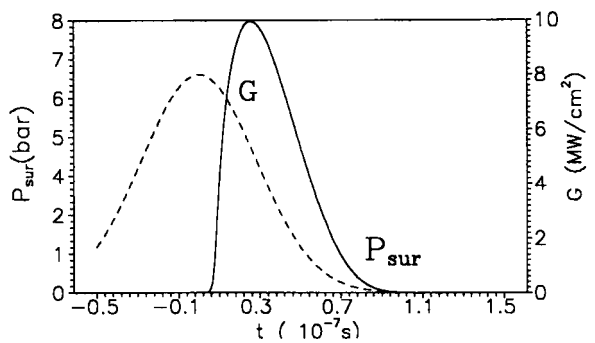

FIG. 13. Intensity of laser pulse G and recoil reactive pressure P_{sur} vs time for volume energy absorption (l_ν=3000 A).

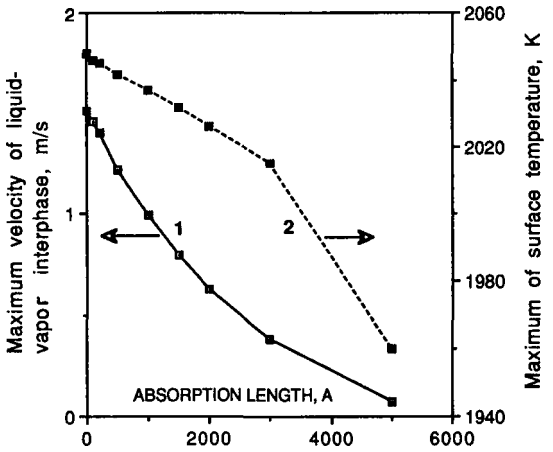

FIG. 14. Maximum values (during thermocycle) of surface temperature T_{sur} (curve 1) and evaporation front velocity V_{kv} (curve 2) vs absorption length.

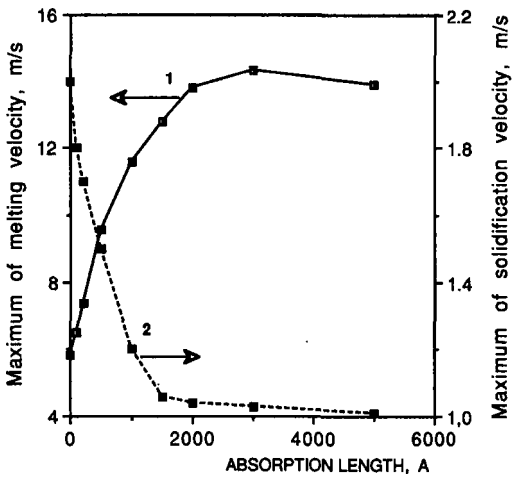

FIG. 16. Maximum absolute values (during thermocycle) of melting $V_{sl}<0$ (curve 1) and solidification $V_{sl}>0$ (curve 2) velocities vs absorption length.

curve 1 in Fig. 14 for $l_\nu=3000$ A. Other parameters (G_0, τ, and heat-transfer properties) of the material remain unchanged.

In the case of surface absorption, $l_\nu=0$, phase transitions are connected with only one metastable state, namely, overheating of the surface being evaporated. In this regime the highest evaporation rates $|V_{kv}^{max}|\approx 1.5$ m/s, Fig. 14, and the highest solidification rates $|V_{sl}^{max}|\approx 2$ m/s, Fig. 16, are found, and the strongest loss of the material due to evaporation $\Delta x_v^{max} \approx 800$ A, Fig. 15, is observed (Δx_v: thickness of evaporated layer per pulse). Melting has the lowest rate, Fig. 16. The ratio of phase front velocities determines the melt thickness, Fig. 17, and the lifetime of the liquid phase.

Overheating of both phases results from the kinetic energy of the phase transformations. The overheating parameters are determined by the rates V_{kv}, V_{sl}, and heat-transfer and optical properties of the material. The maximum values of volume overheating for the solid and liquid phases $\Delta T_{s,l}^{max}$ (Fig. 18), their depths $\Delta x_{s,l}$ (Fig. 19), and time of existence $\Delta t_{s,l}^{ex}$ (Fig. 20) are calculated. The positions of subsurface temperature maxima $\Delta x_{s,l}$ (Δx_l: relatively irradiating surface; Δx_s: relatively solid-liquid interface) were determined at the moments corresponding to the maximum overheating values shown in Fig. 18.

As noted previously, the solid phase overheating ΔT_s is formed by volume energy absorption and the melting process. Elementary estimation based on the boundary condition on solid-liquid interface indicates that its value increases with the increasing mean free path l_ν: $\Delta T_s \sim L_m V_{sl} l_\nu/\lambda$. The increased overheating in turn causes an additional acceleration of melting. As a result all the values characterizing the overheating of the solid phase have a tendency to increase with increasing l_ν (Figs. 18–20). The maximum values are reached for the maximum l_ν value from the considered interval $l_\nu=5000$ A ($\kappa_v=2\times10^4$ cm^{-1}): $\Delta T_s^{max} = 155$ K, $\Delta x_s=800$ A, $\Delta t_s^{ex} \approx 60$ ns. In experiments an explosive decay of the metastable state in solid phase can lead to an ejection of the mixture of solid particles and liquid droplets.

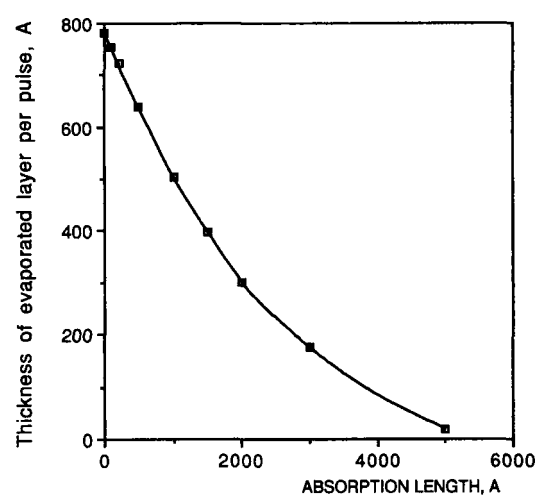

FIG. 15. Thickness of evaporated layer per pulse Δx_v vs absorption length.

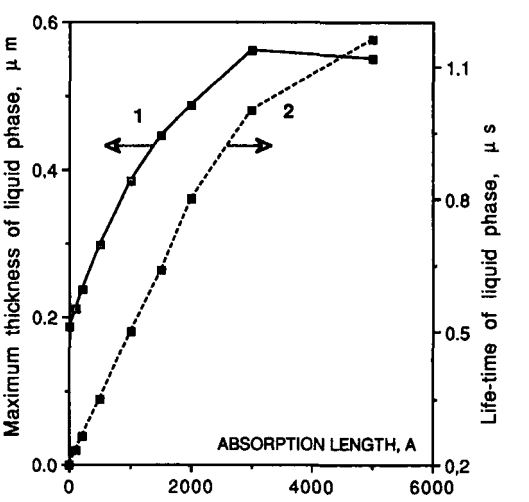

FIG. 17. Maximum thickness of liquid phase Δx_l (curve 1) and its lifetime t_l^{ex} (curve 2) vs absorption length.

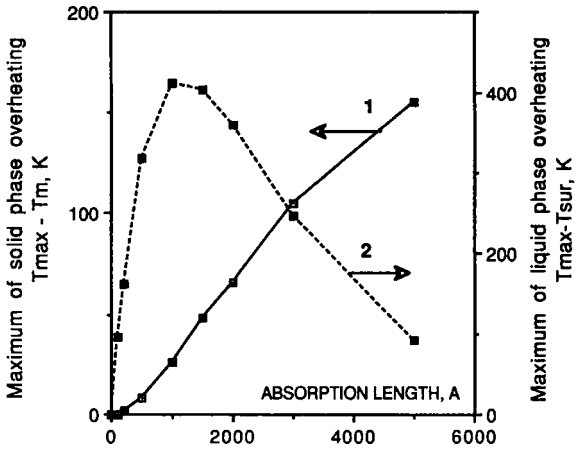

FIG. 18. Maximum values of solid $\Delta T_s = T_{max} - T_m$ (curve 1) and liquid $\Delta T_l = T_{max} - T_{sur}$ (curve 2) phase overheating vs absorption length.

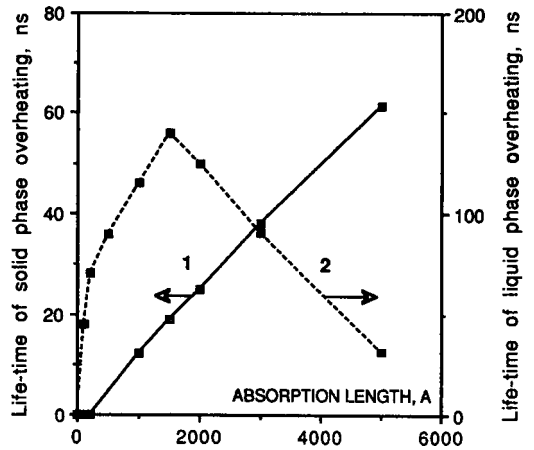

FIG. 20. Lifetime of solid (curve 1) and liquid (curve 2) phase overheating vs absorption length.

At the same time, the increase of the energy releasing area causes a reduction of the surface temperature T_{sur}, and, as a consequence, a reduction of the evaporation rate V_{kv}, Fig. 14. Thus, two main parameters creating the volume overheating of the liquid phase act in the opposite directions. The calculation showed that the possible acceleration due to the liquid metastable state (i.e., subsurface temperature maximum that causes heat flux from the bulk of material toward the surface) cannot compensate the reduction of the evaporation rate caused by the lowered surface temperature. As a result all the dependencies (Figs. 18–20) describing the volume overheating of the liquid $\Delta T_l^{max}(l_v)$, $\Delta x_l(l_v)$, $\Delta t_l^{ex}(l_v)$ in the range of l_v=1000–3000 A have the extreme values: $\Delta T_l^{max}(l_v = 1000\ \text{A}) \approx 400$ K, $\Delta x_l(l_v$=3000 A) ≈ 0.1 μm, $\Delta t_l^{ex}(l_v = 1500\ \text{A}) \approx 140$ ns. So, in the range of laser wavelength $\lambda_v \approx 0.4$–0.6 μm (which corresponds to l_v=1000–3000 A) high values of the temperature ΔT_{sur}^{max} and of the time of existence Δt^{ex} of the overheating increase greatly the probability of an explosive decay of the metastable phase. In experiments this effect can occur as an ejection of material in the form of droplets.

To avoid the above-mentioned extreme overheating values in solid and liquid phases in PLD of ceramics, one needs to use lasers whose irradiation absorption length is smaller than 200 A. In the present case, this corresponds to a laser wavelength $\lambda_v \leqslant 0.2$ μm.

Analysis of the dependencies of the surface temperature $T_{sur}(t)$, and of the rates of evaporation V_{kv}^{max} (Fig. 14), melting ($V_{sl}<0$), and solidification ($V_{sl}>0$), Fig. 16, shows that for volume energy release with $l_v \geqslant 1000$ A melting becomes dominant, which ultimately determines unusually long times of existence of the liquid phase $\Delta t_l^{ex}(l_v = 5000\ \text{A}) \approx 1.2$ μm, Fig. 17. Calculations show also that in the nanosecond range of action the liquid phase depth does not exceed 0.6 μm, Fig. 17, which is clearly insufficient for realization of a developed hydrodynamic motion and related hydrodynamic instability. This supports the assumption that one of the main reasons for the emergence of unstable regimes in PLD of superconducting ceramics is associated with metastable states in solid and liquid phases.

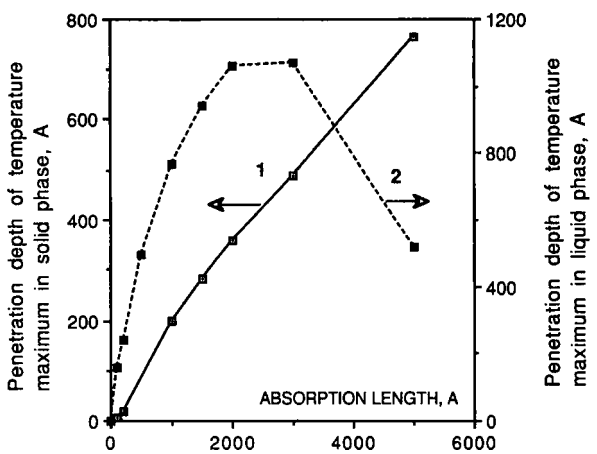

FIG. 19. Positions of temperature maximums in solid phase relative to solid-liquid interface (curve 1) and in liquid phase relative to irradiated surface (curve 2) vs absorption length.

D. Discussion

Different types of cw and pulsed lasers are widely applied in ceramics elaboration and machining. The elaboration of high-T_c (high critical temperature) superconductors is one of the typical examples. These techniques include PLD, thin-film patterning, surface remelting, micromachining, and some others.

One of the most important problem of technology of high-temperature superconducting ceramics elaboration is the increase of critical density of electrical current. The current density is restricted particularly because of the presence of imperfections and grain boundaries. In this connection production of volume monocrystal samples becomes increasingly important.[48] The influence of imperfections and grain boundaries can be eliminated by several methods, such as surface remelting or growth of high-T_c superconducting films from the melt.[48]

Typically Nd-YAG lasers (λ_ν=1.06 μm) and eximer lasers ArF (λ_ν=0.193 μm), KrF (λ_ν=0.248 μm), XeCl (λ_ν=0.308 μm) with energy fluence E=1–10 J/cm^2 and pulse duration τ=1–50 ns are used in ceramics processing.

For determination of optimal regimes for laser surface remelting, PLD and some others should be performed on the basis of comparing theoretical results with experimental data. The main difficulty is just a complete absence of direct measurements concerned with processes in condensed medium (temperature fields in solid and liquid phases, phase front dynamics). The real-time measurements of PLD processes are realized mainly for the plume diagnostic,[49–54] i.e., phenomena in gas phase. The only realistic way is to compare simulation results with general tendencies and indirect measurements.[1–3,55]

As the analysis of experimental data showed, the variation of character of laser-ceramics interaction with radiation wavelength can be used as one of the general tendencies. This behavior is typical for both regimes of laser evaporation without plasma formation[3,55] and with plasma formation based on the evaporated substance.[56] It is usually mentioned[55] that the evaporation process is more stable and the quality of deposited ceramic films is higher for short-wavelength lasers (λ_ν=0.197–0.308 μm) by comparison with irradiation at λ_ν=0.532 μm and λ_ν=1.06 μm. It should be noted that the final achievement of PLD has been reached only with the appearance of eximer lasers such as ArF, KrF, and XeCl.[49–53,57,58] Nd-YAG laser applications on the main λ_ν=1.06 μm and double frequency λ_ν=0.532 μm are narrowed by the stability of surface evaporation. Stability violation results in emergence of liquid droplets[19,55] and solid particles[19,59] in vapor flux, which is probably connected with microexplosions in irradiation zone. The direct connection between the appearance of microcrators on the surface of laser-irradiated ceramics and the sharp decrease of PLD quality has been observed in Ref. 55.

Removal of liquid and solid particles from the evaporated surface in the nanosecond range of laser action can be identified with the explosionlike decay of overheated metastable states. As it follows from the performed analysis, the probability of this decay increases with λ_ν. Well-known advantages of short-wavelength eximer lasers are balanced yet by essentially higher (by one order of magnitude) productivity of Nd-YAG lasers at λ_ν=1.06 μm in PLD.[60]

The theoretical analysis in the present article was performed under some assumptions that idealize to a certain extent the considered situation. The main following assumptions are concerned: The imperfections and grain boundaries are neglected; the thermophysical and optical properties do not vary with temperature. The reasonable question is whether the predicted phenomena such as solid phase overheating and so on are realized in typical experimental conditions.

The performed analysis is relevant to monocrystal as well as to polycrystal materials with characteristic grain sizes larger than thermal influence length l_T. For a wide range of ceramics and nanosecond range of laser pulse duration $l_T \sim 1$ μm. The typical grain size of polycrystal ceramics is about 10–50 μm.

The extrapolation of experimental data from the temperature range 300–1300 K to higher temperatures shows that thermal dependencies of specific heat c_p, thermal conductivity λ_ν, and absorption coefficient κ lead to about 30% variation of these quantities. Such variations can lead to some quantitative deviations from the obtained solution but cannot cause qualitative changes.

More essential influence on simulation results can be expected from possible jump variations of optical and thermophysical characteristics at phase transition. Note that at present there are no evident experimental confirmations of this phenomenon. Moreover, the results of some experiments, devoted to surface modification of ceramics by laser treatment with $G=(3–4)\times10^7$ W/cm^2, τ=50 ns at λ_ν=1.06 μm,[61] showed that laser melting and subsequent rapid crystallization of melt takes place without significant modification of phase composition. At laser action of a few tens of nanoseconds, oxygen does not have enough time to leave the melted layer. The above-mentioned results suggest that thermophysical and optical properties of ceramics change moderately under melting and crystallization.

Therefore, the simulation results obtained under simplified assumptions may be used for experimental data interpretation as well as for determination of optimal regimes for laser material treatment.

V. CONCLUSION

The theoretical analysis performed within the framework of the admitted assumptions provides peculiarities of laser influence on ceramics in the nanosecond range of duration and establishes a qualitative change in the behavior of the processes in the irradiation zone with a change of quantum mean free path.

Volume energy release in ceramics should be taken into account not only for liquid phase, but for solid phase as well, at least at the initial stage of phase front propagation. The ceramics melt becomes optically thick within 10–50 ns for interface velocity $V_{sl} \sim 10–15$ m/s.

The numerical simulation showed that pulsed laser evaporation of materials with volume energy release leads to volume overheating of both solid and liquid phases. The maximum values of the solid phase overheating exceed 100 degrees and those for the liquid phase exceed several hundred degrees for the considered values of the intensity $G=10^7$ W/cm^2, pulse duration τ=40 ns, and pulse temporal profile $G(t)=G\exp[-(t/\tau)^2]$. The lifetimes of the metastable states are tens and hundreds of nanoseconds, respectively. The metastability of the solid phase leads to the domination of the melting process which, together with a decreasing effect of evaporation and low solidification rates, makes the liquid phase lifetime 5–6 times longer than for the surface absorption of radiation. It is shown that the probability of explosive decay of the metastable states in the solid phase increases with laser wavelength, whereas in the liquid phase the corresponding variables exhibit a maximum versus laser wavelength.

From the experimental data related to PLD of superconducting ceramics[1–5] it is known that in order to realize stable evaporation regimes (without droplets, etc....), it is preferable

to use lasers with short wavelengths, for example, λ_ν=0.2–0.4 μm (l_ν=100–500 A), whose dissipation mechanism is close to the surface one. On the contrary, for Nd:YAG (λ_ν=1.06 μm) and CO_2 lasers (λ_ν=10.6 μm) it is practically impossible to obtain the required quality of deposition, because of micron-sized particle generation. The proposed analysis of heat processes in PLD probably explains this tendency.

The analysis performed here is relevant not only to superconducting ceramics, but may be extended (under certain conditions) to a general case of energy flux action on materials with volume energy absorption.

[1] K. Hubler and G. Editor, MRS Bull. **17**, 26 (1992).
[2] J. Cheung and J. Horwitz, MRS Bull. **17**, 30 (1992).
[3] E. Fogarassy, C. Fuchs, S. de Unamuno, J. Perriere, and F. Kerherve, Mater. Manufact. Processes **7**, 31 (1992).
[4] Z. M. Zhang, B. I. Choi, T. A. Le, M. I. Flik, M. P. Siegal, and J. M. Phillips, J. Heat Transfer **114**, 644 (1992).
[5] D. B. Chrisey and A. Inam, MRS Bull. **17**, 37 (1992).
[6] J. C. Maxwell, in *Scientific Papers*, edited by W. D. Niven (Dover, New York, 1965).
[7] M. Volmer, *Kinetik der Phasenbildung* (Leipzig, 1939).
[8] W. Gibbs, *The Scientific Papers* (Dover, New York, 1961), Vol. 1.
[9] *Modern Crystallography: Crystals Formation*, edited by B. K. Vanshtein (Nauka, Moscow, 1980), Vol. 3.
[10] F. Spaepen and D. Turnbull, in *Laser Annealing of Semiconductors*, edited by by J. M. Poate and J. W. Mayer (Academic, New York, 1982), p. 151.
[11] K. A. Jackson, in *Treatise on Solid State Chemistry*, edited by N. B. Hannay (Plenum, New York, 1975), Vol. 5, p. 233.
[12] J. Y. Tsao, M. J. Aziz, M. O. Tompson, and P. Peercy, Phys. Rev. Lett. **56**, 2712 (1986).
[13] M. D. Klude and J. R. Ray, Phys. Rev. B **39**, 1738 (1989).
[14] C. J. Tymczak and J. R. Ray, Phys. Rev. Lett. **64**, 1278 (1990).
[15] P. V. Breslavskii, V. I. Mazhukin, and A. A. Samokhin Sov. Phys. DAN **320**, 1088 (1991).
[16] D. J. Broer and L. Vriens, Appl. Phys. A **32**, 107 (1983).
[17] P. Kivits, R. D. Bont, and P. Zalt, Thin Solid Films **87**, 215 (1982).
[18] A. G. Gorelik, N. V. Dubinin, V. I. Mazhukin, and H. A. Muzafarov (unpublished).
[19] D. L. Lin, X. Li, Z. D. Liu, and T. F. Georgy, J. Appl. Phys. **72**, 4227 (1992).
[20] J. Christian, *Transformation Theory in Metals and Alloys* (Mir, Moscow, 1978), Vol. 1.
[21] J. I. Frenkel, *The Kinetic Theory of Liquids* (Dover, New York, 1955).
[22] S. Williamson, C. Mourou, and J. C. H. Li, Phys. Rev. Lett. **52**, 2364 (1984).
[23] G. I. Alferov, Yu. V. Kovalchuk, Yu. V. Pogorelsky, and O. V. Smolsky, Rep. Belorus Acad. Sci. Phys. Ser. **49**, 1069 (1985).
[24] *Proceedings of the Institute of General Physics Academy of Sciences of the USSR. Effect of Laser Radiation on Absorbing Condensed Matter*, edited by A. M. Prokhorov (Nova Science, Commuck, NY, 1990).
[25] P. K. Wu, AIAA J. **15**, 1809 (1977).
[26] M. W. Sigrist and F. K. Kneubuhl, J. Acoust. Soc. Am. **64**, 1652 (1978).
[27] A. A. Samokhin and A. B. Uspensky, Phys. Rev. Lett. **73**, 391 (1979).
[28] V. P. Skripov, *Metastable Liquids* (Israel Program for Scientific Translation, Jerusalem, 1974).
[29] H. S. Carslaw and J. C. Jaeger, *Conduction of Heat in Solids* (Clarendon, Oxford, 1964).
[30] L. D. Landau, and E. M. Lifshits, *Statistical Physics* (Pergamon, London, 1958).
[31] K. A. Jackson, in *Surface Modification and Alloying by Laser, Ion and Electron Beams*, edited by J. M. Poate, G. Foti, and D. C. Jacobson (Plenum, New York, 1983), p. 51.
[32] J. Q. Broughton, G. H. Gilmer, and K. A. Jackson, Phys. Rev. Lett. **49**, 1496 (1982).
[33] J. J. Masters, J. Appl. Phys. **27**, 477 (1956).
[34] D. Crout, J. Math. Phys. **15**, 1 (1936).
[35] S. I. Anisimov, Y. A. Imas, G. S. Romanov, and Yu. V. Hodyko, *Action of High Power Laser Radiation on Metals* (Nauka, Moscow, 1970).
[36] C. J. Knigt, AIAA J. **17**, 519 (1979).
[37] H. Aden, E. Beyer, and G. Herziger, J. Phys. D **23**, 655 (1990).
[38] N. A. Dar'in and V. I. Mazhukin, Differencialnie Uravnenija **23**, 1154 (1987).
[39] N. A. Dar'in and V. I. Mazhukin, DAN USSR **298**, 64 (1988).
[40] V. I. Mazhukin and L. Yu Takoeva, Matematicheskoje Modelirovanije **2**, 101 (1990).
[41] P. V. Breslavskij, V. I. Mazhukin, and L. Yu Takoeva (unpublished).
[42] V. I. Mashukin, U. Semmler, P. V. Breslavskij, and L. Ju. Takoeva (unpublished).
[43] V. I. Mashukin, U. Semmler, P. V. Breslavskij, and L. Ju. Takoeva (unpublished).
[44] R. K. Williams, R. S. Graves, D. M. Kroeger, G. C. Marsh, J. O. Scarbrough, and J. Brynestad, J. Appl. Phys. **66**, 6181 (1989).
[45] J. Orenstein, G. A. Thomas, F. J. Millis, S. L. Cooper, D. H. Rapkine, T. Timusk, L. F. Schneemeyer, and J. V. Waszczak, Phys. Rev. B **42**, 6342 (1990).
[46] K. E. Goodson and M. I. Flik, J. Heat Transfer **115**, 17 (1993).
[47] A. Lashin, I. Smurov, A. Uglov, P. Matteazzi, and V. Tagliferri, Int. J. Heat Technol. **7**, 60 (1989).
[48] L. I. Demjanetcz, Usp. Phys. Sci. **161**, 71 (1991).
[49] P. E. Dyer, R. D. Greenough, A. Issa, and P. H. Key, Appl. Phys. Lett. **53**, 534 (1989).
[50] C. Girault, D. Damiani, J. Aubreton, and A. Catherinot, Appl. Phys. Lett. **55**, 182 (1989).
[51] R. K. Singh, O. W. Holland, and J. Narajan, J. Appl. Phys. **68**, 233 (1990).
[52] X. D. Wu, B. Dutta, M. S. Hegle, A. Inam, T. Venkatesan, E. W. Chase, C. C. Chang, and R. Howard, Appl. Phys. Lett. **54**, 179 (1989).
[53] R. K. Singh and J. Narajan, Phys. Rev. B **41**, 8843 (1990).
[54] A. Cupta, J. Appl. Phys. **73**, 7877 (1993).
[55] V. Craciun, S. Amirahaghi, D. Craciun, J. Elders, J. G. E. Gardeniers, and I. W. Boyd, Appl. Surf. Sci. (to be published).
[56] J. A. Miehé, Appl. Surf. Sci. (to be published).
[57] C. Girault, D. Damiam, J. Aubreton, and A. Catherinot, Appl. Phys. Lett. **54**, 2035 (1989).
[58] D. B. Geohegan, Appl. Phys. Lett. **60**, 2732 (1992).
[59] T. Venkatesan, C. C. Chang, D. D. Dijkkamp, S. B. Ogale, E. W. Chase, L. A. Farrow, D. M. Hwang, P. E. Miceli, S. A. Schwarz, J. M. Tarascon, X. D. Wu, and A. Inam, J. Appl. Phys. **63**, 4591 (1988).
[60] K. Mukherjee, C. W. Chen, J. Yoo, I. Oh, and S. Kudapa, in *Surface Treatment and Thin Film Deposition*, edited by J. Mazumder, NATO ASI Series, Series E: Applied Sciences (Kluwer, Dordrecht, in press).
[61] V. A. Jesenkin, A. G. Uljashin, I. G. Goralchuk, and Yu. A. Bumad, J. Eng. Phys. (Russia) **61**, 5 (1991).